Int. J. Electrochem. Sci., 7 **(2012)** 2468 - 2486

International Journal of
ELECTROCHEMICAL
SCIENCE
www.electrochemsci.org

Theoretical and Quantitative Structural Relationship Studies of Reorganization Energies of [SWCNT(5,5)-Armchair-C_nH_{20}] (n=20-310) Nanostructures by Neural Network CFFBP Method

Avat Arman Taherpour[*1], *Adeleh Aghagolnezhad-Gerdroudbari*[1] *and Saeid Rafiei*[2]

[1]Chemistry Department, Faculty of Science, Islamic Azad University, P.O. Box 38135-567, Arak, Iran.
[2]Young Researchers Cub, Islamic Azad University, Aligudarz Branch, Aligudarz, Iran.
[*]E-mail: avatarman.taherpour@gmail.com, ataherpour@iau-arak.ac.ir

Received: 17 December 2011 / *Accepted:* 22 January 2012 / *Published:* 1 March 2012

Nanotubes of type (*n*,*n*) are called *armchair nanotubes* because of their "W" shape, which is perpendicular to the tube axis. One primary *armchair nanotube* is the SWCNT(5,5)-armchair. To establish a good structural relationship between the structure of molecules [SWCNT(5,5)-Armchair-C_nH_{20}] (n=20-190) 1-18, the number of carbon atoms (C_n) as well as the LUMO-HOMO gap (ΔE in eV), absolute hardness (η), adiabatic ionization potential (I_{pa}), vertical ionization potential (I_{pv}), and the LUMO and HOMO energies of 1-18 were used as the numerical and structural properties of these unsaturated compounds. In this study, the relationship between this index with the electron reorganization energy (λ_e) and hole reorganization energy (λ_h) were assessed using the *Marcus* theorem for the predicted SWCNT 1-18. The results were extended for [SWCNT(5,5)-armchair-C_nH_{20}] (n=200-310) 19-30. In addition, the cascade-feed forward back-propagation neural network (CFFBP-NN) method was utilized for modeling.

Keywords: Single-wall Nanotubes; Electron reorganization energy (λ_e); Hole reorganization energy (λ_h); Marcus Theory; Neural Network; Molecular modeling.

1. INTRODUCTION

Nanoscale structures of carbon display an attractive variation of structural characteristics, and many useful forms have been synthesized and identified. Single wall carbon nanotubes (SWCNTs) are among some of the most interesting new materials discovered in many years. Grown catalytically at high temperature in the gas phase, they can almost be structurally perfect and show ballistic electron motion at 23°C over lengths of several micrometers.[1-3] This near structural perfection, coupled with physical rigidity and weak vibronic coupling compared to other conjugated aromatic polymers, makes them ideal for fundamental studies of electrons in one dimension. Infinite length SWNTs are π-bonded

aromatic molecules that can either be semiconducting or metallic, depending on the diameter and helical angle. [1-3] In a pioneering 1992 DFT calculation, Mintmire, Dunlap, and White predicted that the infinite length of the (5,5) armchair SWNT (0.67 nm diameter) would be metallic with a very low transition temperature separating the uniform (high temperature) structure from the Peierls bond, alternating (low temperature) the structure.[1,2] This specific SWNT is the elongated tube of the molecular family of C_{60}, C_{70}, and so on. The electronic structure of SWNTs can also be simply understood using the most elementary topological Hückel (tight-binding) molecular orbital (MO) analysis. [2,3]

SWNTs are highly promising for building miniaturized electronics beyond the scale currently used. [4-8] The one-dimensional (1-D), nanowire-like structure of SWNTs especially has the potential to construct ideal nano-highways for charge carriers on electrodes. Thus, SWNTs have been studied for the use of electron- or hole-transporting materials in photovoltaic and photoelectrochemical devices. [9-29] The most widely studied SWNT-based photovoltaic devices involve a photoactive layer of bulk heterojunction structures, in which SWNTs are blended with electron-donating, π-conjugated polymers, such as poly(*p*-phenylenevinylene) and polythiophene. [15-18] In such cases, SWNTs are expected to act as electron-transporting pathways and electron acceptors. In addition, individual SWNTs provide a large surface area at the polymer-SWNT interface, which would be favorable for the efficient dissociation of excitations. [4]

Nanotubes of type (*n*,*n*) are called *armchair nanotubes* because of their "W" shape, which is perpendicular to the tube axis. They are symmetrical along the tube axis with a short unit cell (0.25 nm or 2.5 Å) that is repeated along the entire section of the long nanotube. All other nanotubes are called *chiral nanotubes* and have longer unit cell sizes along the tube axis.[1,30,31] The simplest type of nanotube is a cylindrical structure, which could conceptually be formed by the folding and gluing of one pair of opposite sides of a rectangular graphite sheet [1,30-45]. If both ends are capped, the nanotube will have at least two pentagons and, therefore, be a type of fullerene. Nanotubes are large, linear fullerenes with aspect ratios as large as 10^3 to 10^5 [31]. The walls of such tubes could exhibit various sizes of polygons.[46-48] Although many nanoscale fullerene materials occur regularly in applications, the controlled production of many fullerenes and nanotubes with well-defined characteristics has not yet been achieved.[37-39, 46-48] Because of their properties, they can act as lightweight, large surface-area packing materials for gas storage and hydrocarbon fuel storage devices, nanoscale devices for molecular drug delivery and as casting structures for making nanowires and nanocapsulates. Exceptionally strong nanotubes can be used to make lightweight structural materials. Nanotubes, such as "*capsulates"* can help store and carry hydrogen and other hydrocarbon-based fuel in engines or aboard spacecraft. These important groups of carbon allotropes can be easily closed on both sides. Single-wall carbon nanotubes are among the most interesting new carbon allotropes that have been discovered in many years [1,30].

Carbon nanotubes possess many special properties, such as an open mesoporous structure, high electrical conductivity and chemical stability, as well as extremely high mechanical strength and modulus [31, 40-43]. These properties aid in the transportation of ions and facilitate the charge of the double layer as well as present advantages in the development of electrochemical capacitors [43].

Single-walled carbon nanotubes have been recognized as potential electrode materials for electrochemical capacitors [43-45].

One of the most widely recognized structures of nanotubes is the (5,5) tube. The structure of the (5,5) tube can be built by successively adjoining sections of 10 C atoms. In the infinite tube, the periodic unit cell is composed of two such sections consisting of 20 C atoms [1]. The electronic structures and electrical properties of single wall nanotubes can be simulated from a layer of graphite (graphene sheet) [40-44].

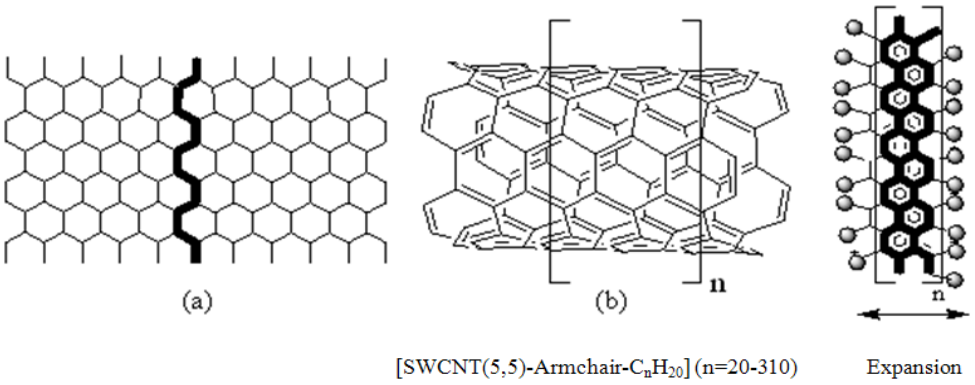

Figure 1. (a) The expanded form and (b) the structures that were investigated are as follows: $C_{20}H_{20}$ **(1)**,$C_{30}H_{20}$ **(2)**,$C_{40}H_{20}$ **(3)**,$C_{50}H_{20}$ **(4)**,$C_{60}H_{20}$ **(5)**,$C_{70}H_{20}$ **(6)**,$C_{80}H_{20}$ **(7)**,$C_{90}H_{20}$ **(8)**,$C_{100}H_{20}$ **(9)**,$C_{110}H_{20}$ **(10)**,$C_{120}H_{20}$ **(11)**,$C_{130}H_{20}$ **(12)**,$C_{140}H_{20}$ **(13)**,$C_{150}H_{20}$ **(14)**,$C_{160}H_{20}$ **(15)**,$C_{170}H_{20}$ **(16)**,$C_{180}H_{20}$ **(17)** and $C_{190}H_{20}$ **(18)**.

Figure 1 shows the (5,5) *armchair* form and the imaginary structures of the [SWCNT(5,5)-armchair-C_nH_{20}] n=20-310). In experiments, the nanotubes may not contain any hydrogen atoms (there is no hydrogen in the electric arc technique), and the nanotubes can be easily closed at both ends.

The electronic structures of tubular aromatic molecules derived from the metallic (5,5) armchair SWCNT for $C_{20}H_{20}$ up to $C_{210}H_{20}$ (see Figure 1) were reported by Zhou et al. in 2004 [1]; that report considered how the electronic structures of short molecular sections of the (5,5) tube related to, differed from, and asymptotically approached those of an infinite metallic tube [1]. Some of the structural and electronic properties were investigated, such as the ionization potential, electron affinity, Fermi energy (E_f), chemical hardness, and relative energetic stability. All of these parameters exhibited the length periodicity, which was also seen in the frontier orbital (FO, i.e., HOMO-LUMO: Highest Occupied Molecular Orbital–Lowest Unoccupied Molecular Orbital) gap, in contrast to the optical "charge transfer" transition and the static axial polarizability [1]. These (5,5) nanotubes have two types of symmetry; for nanotubes with odd identification numbers (1-17 odd numbers), the point group is D_{5d}, and for nanotubes with even identification numbers (2-18 even numbers), the point group is D_{5h}. In that study, static and TD-DFT (Time Dependent–Density Function Theory) were independently used to optimize the structure for neutral, cationic and anionic complexes [1]. The hybrid non-local B3LYP (Becke, three-parameter, Lee-Yang-Parr) functional was applied [1].

Infinite length SWCNTs are π-bonded aromatic structures that can be either semi-conducting or metallic, depending on the diameter and helical angle of the SWCNTs. In a pioneering 1992 DFT calculation, Mintmire et al. predicted that the infinite length (5,5) armchair SWCNT (6.70 Å diameter) would be metallic with a very low transition temperature separating the uniform (high temperature) structure from the Peierls bond alternating (low temperature) structure [35,37]. This specific SWCNT is the elongated tube of the molecular family of C_{60}, C_{70}, and so on [1].

Graph theory has been determined as a useful tool in assessing the *QSAR* (Quantitative Structure Activity Relationship) and *QSPR* (Quantitative Structure Property Relationship) [46-62]. Considerations based on a Quantitative Structural Analysis Relationship Study (QSARS) must be taken into account when extrapolating results of one compound to another; this process primarily depends on how close the physical and chemical properties are of the compounds in question [63,64]. Numerous studies in the above areas have also utilized topological indices (TI) [65-68]. It is important to use effective mathematical methods to make strong connections between the data corresponding to several chemical properties. One of the most useful numerical and structural values of unsaturated compounds, such as in nanotubes, is the degree of unsaturation (D_U). This quantity is a useful index for determining the number of cyclic structures and/ or π-bonds in a molecule. [50-64] In previous studies, the relationship between the D_U index, the electron affinity, the reduction potential ($^{Red.}E_1$) of [SWCNT(5,5)-armchair-C_nH_{20}] and the free energy of electron transfer (ΔG_{et}) between [SWCNT(5,5)-armchair-C_nH_{20}] structures and fullerene C_{60} (as C_{60}@[SWCNT(5,5)-armchair-C_nH_{20}] complexes) was investigated [50]. The relationship between the D_U index and the free energy of electron transfer (ΔGet), which was assessed using the Rehm-Weller equation on the basis of the first oxidation potential ($^{ox}E_1$) of Sc_2@C_{84} and Er_2@C_{82} for the predicted supramolecular complexes between and the endohedral metallofullerenes Sc_2@C_{84} and Er_2@C_{82} as [M_2@C_x]@[SWCNT(5,5)-Armchair-C_nH_{20}] (M = Er and Sc, x=82 and 84), have been presented and discussed in previous studies [63,64].

In a study on the structural properties of [SWCNT(5,5)-armchair-C_nH_{20}] (n=20-190) 1-18, the relationship among the number of carbon atoms of the SWCNT (C_n) index, the gap between the LUMO-HOMO states (ΔE in eV), the absolute hardness (η), the adiabatic ionization potential (I_{pa}), the vertical ionization potential (I_{pv}), the LUMO and HOMO energies of 1-18 to calculate the electron reorganization energy (λ_e) and the hole reorganization energy (λ_h), as assessed using the *Marcus* theory on the basis of the electron transfer process, were investigated. These results have been extended to [SWCNT(5,5)-armchair-C_nH_{20}] (n=200-310) 19-30. Marcus's theory builds on the traditional *Arrhenius* equation for the rates of chemical reactions in two ways. First, it provides a formula for the pre-exponential factor in the *Arrhenius* equation, which is based on the electronic coupling between the initial and final state of the electron transfer reaction (i.e., the overlap of the electronic wave functions of the two states). Second, it provides a formula for the activation energy, which is based on a parameter called the *reorganization energy* and the *Gibbs* free energy. The *reorganization energy* is defined as the energy required to reorganize the structure of the system from the initial to the final coordinates, without changing the electronic state.[69-78]

2. GRAPHING AND MATHEMATICAL METHODS

The number of carbon atoms (C_n), as a structural index for compounds (1-18 and 19-30), were analyzed along with the LUMO-HOMO gap (ΔE in eV), absolute hardness (η), adiabatic ionization potential (I_{pa}), vertical ionization potential (I_{pv}), LUMO and HOMO energies of 1-18. After some mathematical operations, the results were obtained and are shown in the tables and figures for [SWCNT(5,5)-Armchair-C_nH_{20}] (n=20-190) nanotubes 1-18.[1]

All graphing and mathematical operations were performed using the *MATLAB-7.8.0.347(R2009a)* and *Microsoft Office Excel-2007* software programs. The number of carbon atoms (C_n), the LUMO-HOMO gap (ΔE in eV), absolute hardness (η), adiabatic ionization potential (I_{pa}), vertical ionization potential (I_{pv}), and LUMO and HOMO energies of 1-18 are very useful numerical and structural values for the application of the model. The cascade-feed forward back-propagation neural network (CFFBP-NN) models were examined in this study to calculate the electron reorganization energy (λ_e) and the hole reorganization energy (λ_h). Some other indices were examined; however, only the best results and equations for extending the physicochemical and electrochemical data were chosen.

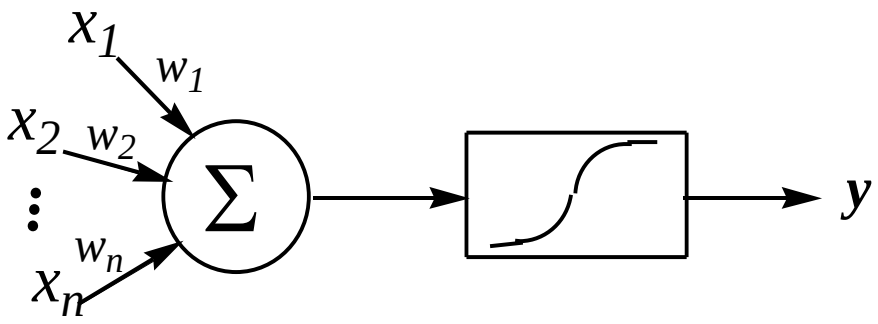

Figure 2. The block diagram of a simple neuron.

A neural network is an information processing system that is composed of an interconnected assembly of simple processing units called neurons [79]. Each neuron has a non-linear transfer function (activation function) and is connected to other neurons via weighted interconnections. Figure 2 is a block diagram of a simple neuron showing the input signals {x_1, x_2,…, x_n}, the weighted interconnects {w_1, w_2,…, w_n}, and the non-linear activation function. A common activation function is the sigmoid. See Figure 2.

$$y = f(a) = \frac{1}{1+e^{-a/p}} \qquad \text{(Eq. 1)}$$

The *"a"* is the sum of the weighted interconnections to a particular neuron and is given by the following equation:

$$a = \sum_{i=1}^{n} w_i\, x_i \qquad \text{(Eq. 2)}$$

The weighed interconnections $\{w_1, w_2, \ldots, w_n\}$, are determined by training the neural network. A neural network is trained by using a known set of input and output patterns. A known input pattern is applied to the neural network and subsequently, the weighed interconnections are adjusted until the output of the neural network matches the desired output, within a certain tolerance.[79]

Trained neural networks have several properties that make them attractive for use in crack dimension estimation problems. These properties include the following [79]:

1) The ability to generalize from the training set.

2) The output signal is insensitive to noise appearing at its inputs.

3) Trained neural networks have fast execution times.

The Marcus theory of electron transfer implies a rather weak (<0.05 eV) electronic coupling interaction between the initial (locally excited, LE) and final (electron transfer, ET) states; in addition, it presumes that the transition state is close to the crossing point of the LE and ET terms. The value of the electron transfer rate constant k_{et} is controlled by the activation free energy $\Delta G^{\#}_{et}$, which is a function of the reorganization energy (l/4) and the electron transfer driving force ΔG_{et}. For organic molecules, the reorganization energy was found to be in the range 0.1-0.3 eV.[69-76] The small reorganization energy leads to an acceleration of the charge separation (CS), and the deceleration of the charge recombination (CR) is processed as expected from the Marcus theory of electron transfer. [77,78,80] The rate of CR can be clearly slowed by shifting deep into the inverted region of the Marcus parabola, where the driving force ($-\Delta G_{et}^{\circ}$) is larger than the total reorganization energy (λ) of electron transfer.[77,78,80] Extensive efforts have been directed towards establishing the driving force dependence of rate constants for the electron transfer and thereby probing the Marcus inverted region where the electron-transfer rate decreases with increasing the driving force of electron transfer. [80-90]

3. RESULTS AND DISCUSSION

The Marcus theory is currently the dominant theory of electron transfer in chemistry. The Marcus theory is widely accepted because it makes surprising predictions about electron transfer rates that have been supported experimentally over the last several decades. The most significant prediction is that the rate of electron transfer will increase as the electron transfer reaction becomes more exergonic, but only to a certain point. [69-78,80-90]

Electron transfer (ET) is one of the most important chemical processes in nature, and it plays a central role in many biological, physical and chemical (both organic and inorganic) systems. Solid-state electronics depend on the control of the ET in semiconductors, and the new area of molecular electronics depends critically on understanding and controlling the transfer of electrons in and between molecules and nanostructures. The other reason to study electron transfer is that it is a very simple type of chemical reaction, which once understood, can provide insight into other types of chemical and biochemical reactions. After all, chemistry is basically the transfer of electrons from one place to another. [69-78,80-90]

The free energy of electron transfer ΔG_{et} is the difference between energy values of the reactants on the left and the products on the right; the value of $\Delta G_{et}^{\#}$ represents the activation energy.

Reorganization energy is the energy it would take to force the reactants to have the same nuclear configuration as the products, without permitting the electron transfer. If the entropy changes are ignored, the free energy becomes energy or potential energy. [69-78,80-90]

Table 1. The selected *"Input"* data of [SWCNT(5,5)-Armchair-C_nH_{20}] (n=20-190) 1-18 for calculation the electron reorganization energy (λ_e) by the neural network model. See Ref.[1].

	$C_{20}H_{20}$	$C_{30}H_{20}$	$C_{40}H_{20}$	$C_{50}H_{20}$	$C_{60}H_{20}$	$C_{70}H_{20}$	$C_{80}H_{20}$	$C_{90}H_{20}$	$C_{100}H_{20}$
LUMO-HOMO gap Δ	3.58	2.48	3.04	2.21	1.56	2.20	1.73	1.11	1.70
absolute hardness η	6.31	5.08	5.50	4.51	3.75	4.31	3.73	3.04	3.56
adiabatic ionization potential I_{pa}	6.27	5.73	5.96	5.47	5.17	5.48	5.24	4.94	5.23
vertical ionization potential I_{pv}	6.39	5.87	6.07	5.54	5.27	5.56	5.28	4.98	5.25
LUMO	-1.44	-2.08	-1.79	-2.18	-2.61	-2.30	-2.55	-2.91	-2.63
|HOMO|	5.02	4.56	4.83	4.39	4.17	4.50	4.28	4.02	4.32
	$C_{110}H_{20}$	$C_{120}H_{20}$	$C_{130}H_{20}$	$C_{140}H_{20}$	$C_{150}H_{20}$	$C_{160}H_{20}$	$C_{170}H_{20}$	$C_{180}H_{20}$	$C_{190}H_{20}$
LUMO-HOMO gap Δ	1.51	0.88	1.30	1.33	0.73	1.14	1.21	0.70	0.93
absolute hardness η	3.30	2.62	2.99	2.93	2.34	2.65	2.72	2.19	2.37
adiabatic ionization potential I_{pa}	5.09	4.81	4.98	4.99	4.69	4.82	4.92	4.65	4.72
vertical ionization potential I_{pv}	5.14	4.83	5.02	5.00	4.74	4.90	4.95	4.68	4.79
LUMO	-2.74	-3.08	-2.87	-2.88	-3.20	-3.00	-2.98	-3.24	-3.13
|HOMO|	4.24	3.96	4.18	4.21	3.93	4.14	4.19	3.94	4.07

The values of the relative structural coefficients for the SWCNT (5,5) armchair for $C_{20}H_{20}$ up to $C_{190}H_{20}$ ([SWCNT(5,5)-armchair-C_nH_{20}] 1-18), the LUMO-HOMO gap (ΔE in eV), absolute hardness (η), adiabatic ionization potential (I_{pa}), vertical ionization potential (I_{pv}), and LUMO and HOMO energies of 1-18 are shown in Table 1. The values shown in Table 1 for 1-18 exhibited some mathematical structure. The data were utilized to calculate the electron reorganization energy (λ_e) using the *Marcus* theorem for the predicted SWCNT 1-30 by the neural network model.

Table 2. The *"Target"* energy data for [SWCNT(5,5)-Armchair-C_nH_{20}] (n=20-190) 1-18 of the electron reorganization energy (λ_e) by the neural network model.

	$C_{20}H_{20}$	$C_{30}H_{20}$	$C_{40}H_{20}$	$C_{50}H_{20}$	$C_{60}H_{20}$	$C_{70}H_{20}$	$C_{80}H_{20}$	$C_{90}H_{20}$	$C_{100}H_{20}$
electron reorganization energy λ_e	0.260	0.110	0.100	0.110	0.050	0.080	0.060	0.040	0.020
	$C_{110}H_{20}$	$C_{120}H_{20}$	$C_{130}H_{20}$	$C_{140}H_{20}$	$C_{150}H_{20}$	$C_{160}H_{20}$	$C_{170}H_{20}$	$C_{180}H_{20}$	$C_{190}H_{20}$
electron reorganization energy λ_e	0.070	0.030	0.040	0.060	0.030	0.100	0.010	0.030	0.040

Table 3. The *"Test"* data for [SWCNT(5,5)-Armchair-C_nH_{20}] (n=200-310) 19-30 of the electron reorganization energy (λ_e) by the neural network model. See Ref.[1].

	$C_{200}H_{20}$	$C_{210}H_{20}$	$C_{220}H_{20}$	$C_{230}H_{20}$	$C_{240}H_{20}$	$C_{250}H_{20}$
LUMO-HOMO gap Δ	1.17	0.7	0.6932	0.6524	0.6133	0.5759
absolute hardness η	2.59	2.03	2.095	2.027	1.962	1.9
adiabatic ionization potential I_{pa}	4.6791	4.6474	4.6171	4.5882	4.5606	4.5341
vertical ionization potential I_{pv}	4.91	4.63	4.6323	4.6021	4.5732	4.5454
LUMO	-3.02	-3.27	-3.123	-3.1499	-3.1757	-3.2003
|HOMO|	4.20	3.97	3.8163	3.8023	3.789	3.7762
	$C_{260}H_{20}$	$C_{270}H_{20}$	$C_{280}H_{20}$	$C_{290}H_{20}$	$C_{300}H_{20}$	$C_{310}H_{20}$
LUMO-HOMO gap Δ	0.54	0.5055	0.4724	0.4404	0.4095	0.3797
absolute hardness η	1.84	1.783	1.727	1.674	1.623	1.573
adiabatic ionization potential I_{pa}	4.5086	4.484	4.4604	4.4376	4.4155	4.3942
vertical ionization potential I_{pv}	4.5187	4.4931	4.4683	4.4445	4.4214	4.3991
LUMO	-3.224	-3.2467	-3.2686	-3.2896	-3.31	-3.3296
|HOMO|	3.764	3.7522	3.7409	3.73	3.7195	3.7093

Table 2 shows the *"Target"* energy data for [SWCNT(5,5)-Armchair-C_nH_{20}] (n=20-190) 1-18 with the corresponding electron reorganization energy (λ_e) using the neural network model. Table 3 shows the *"Test"* data for [SWCNT(5,5)-Armchair-C_nH_{20}] (n=200-310) 19-30 with the corresponding electron reorganization energy (λ_e) using the model. Table 4 demonstrates the *"Output"* data for the [SWCNT(5,5)-Armchair-C_nH_{20}] (n=200-310) 19-30 with the corresponding electron reorganization energy (λ_e) using the neural network model.

Table 4. The *"Output"* data for [SWCNT(5,5)-Armchair-C_nH_{20}] (n=200-310) 19-30 of the electron reorganization energy (λ_e) by the neural network model (45 LOGSIG, 50 LOGSIG, 1 PURELIN).

	$C_{200}H_{20}$	$C_{210}H_{20}$	$C_{220}H_{20}$	$C_{230}H_{20}$	$C_{240}H_{20}$	$C_{250}H_{20}$
electron reorganization energy λ_e	0.061	0.038	0.072	0.074	0.076	0.078
	$C_{260}H_{20}$	$C_{270}H_{20}$	$C_{280}H_{20}$	$C_{290}H_{20}$	$C_{300}H_{20}$	$C_{310}H_{20}$
electron reorganization energy λ_e	0.080	0.081	0.083	0.084	0.086	0.087

Table 5. The selected *"Input"* data of [SWCNT(5,5)-Armchair-C_nH_{20}] (n=20-190) 1-18 for calculation the hole reorganization energy (λ_h) by the neural network model. See Ref.[1].

	$C_{20}H_{20}$	$C_{30}H_{20}$	$C_{40}H_{20}$	$C_{50}H_{20}$	$C_{60}H_{20}$	$C_{70}H_{20}$	$C_{80}H_{20}$	$C_{90}H_{20}$	$C_{100}H_{20}$
LUMO-HOMO gap Δ	3.58	2.48	3.04	2.21	1.56	2.20	1.73	1.11	1.70
absolute hardness η	6.31	5.08	5.50	4.51	3.75	4.31	3.73	3.04	3.56
adiabatic ionization potential I_{pa}	6.27	5.73	5.96	5.47	5.17	5.48	5.24	4.94	5.23
vertical ionization potential I_{pv}	6.39	5.87	6.07	5.54	5.27	5.56	5.28	4.98	5.25
LUMO	-1.44	-2.08	-1.79	-2.18	-2.61	-2.30	-2.55	-2.91	-2.63
	$C_{110}H_{20}$	$C_{120}H_{20}$	$C_{130}H_{20}$	$C_{140}H_{20}$	$C_{150}H_{20}$	$C_{160}H_{20}$	$C_{170}H_{20}$	$C_{180}H_{20}$	$C_{190}H_{20}$
LUMO-HOMO gap Δ	1.51	0.88	1.30	1.33	0.73	1.14	1.21	0.70	0.93
absolute hardness η	3.30	2.62	2.99	2.93	2.34	2.65	2.72	2.19	2.37
adiabatic ionization potential I_{pa}	5.09	4.81	4.98	4.99	4.69	4.82	4.92	4.65	4.72
vertical ionization potential I_{pv}	5.14	4.83	5.02	5.00	4.74	4.90	4.95	4.68	4.79
LUMO	-2.74	-3.08	-2.87	-2.88	-3.20	-3.00	-2.98	-3.24	-3.13

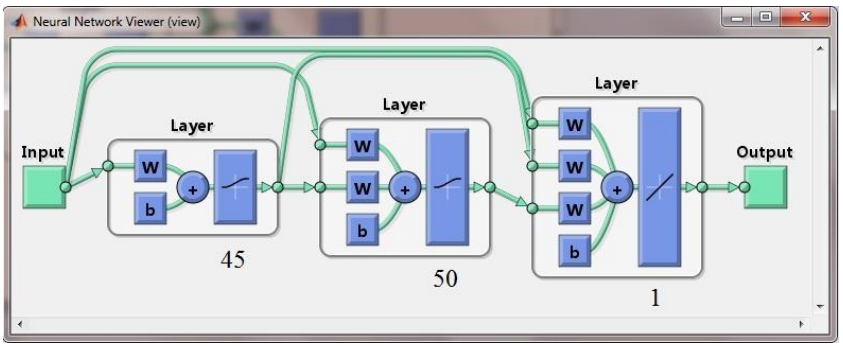

Figure 3. The CFFBP-NN method used to calculate λ_e for 1-30.

The data corresponding to the layers of the neural network model that were used to calculate the electron reorganization energy are as follows: LOGSIG=45, LOGSIG=50 and PURELIN=1 (see Tables 2-4 and Figure 3). From $C_{20}H_{20}$ up to $C_{190}H_{20}$, the point groups alternated between D_{5d} and D_{5h}. To calculate the hole reorganization energy (λ_h), the data from Table 5 were utilized to predict values for SWCNT 1-30 by the neural network model. The LUMO-HOMO gap (ΔE in eV), absolute hardness (η), adiabatic ionization potential (I_{pa}), vertical ionization potential (I_{pv}) and LUMO energy levels of 1-18 are shown in Table 5.

Table 6. The *"Target"* energy data for [SWCNT(5,5)-Armchair-C_nH_{20}] (n=20-190) 1-18 of the hole reorganization energy (λ_h) by the neural network model.

	$C_{20}H_{20}$	$C_{30}H_{20}$	$C_{40}H_{20}$	$C_{50}H_{20}$	$C_{60}H_{20}$	$C_{70}H_{20}$	$C_{80}H_{20}$	$C_{90}H_{20}$	$C_{100}H_{20}$
hole reorganization energy λ_h	0.120	0.140	0.110	0.070	0.090	0.080	0.040	0.040	0.030
	$C_{110}H_{20}$	$C_{120}H_{20}$	$C_{130}H_{20}$	$C_{140}H_{20}$	$C_{150}H_{20}$	$C_{160}H_{20}$	$C_{170}H_{20}$	$C_{180}H_{20}$	$C_{190}H_{20}$
hole reorganization energy λ_h	0.050	0.010	0.040	0.010	0.050	0.080	0.020	0.030	0.070

Table 6 shows the *"Target"* energy data for [SWCNT(5,5)-Armchair-C_nH_{20}] (n=20-190) 1-18 with the corresponding hole reorganization energy (λ_h) calculated by the neural network model. Table 7 shows the *"Test"* data for [SWCNT(5,5)-Armchair-C_nH_{20}] (n=200-310) 19-30 with the corresponding hole reorganization energy (λ_h) calculated by the model. Table 8 demonstrates the *"Output"* data for [SWCNT(5,5)-Armchair-C_nH_{20}] (n=200-310) 19-30 with the corresponding hole reorganization energy (λ_h) by the neural network model. The layers data of the neural network model used to calculate the hole reorganization energy are as follows: LOGSIG=20, TANSIG=40 and PURELIN=1. See Tables 6-8 and Figure 4.

Table 7. The *"Test"* data for [SWCNT(5,5)-Armchair-C_nH_{20}] (n=200-310) 19-30 of the hole reorganization energy (λ_h) by the neural network model.

	$C_{200}H_{20}$	$C_{210}H_{20}$	$C_{220}H_{20}$	$C_{230}H_{20}$	$C_{240}H_{20}$	$C_{250}H_{20}$
LUMO-HOMO gap Δ	1.17	0.7	0.6932	0.6524	0.6133	0.5759
absolute hardness η	2.59	2.03	2.095	2.027	1.962	1.9
adiabatic ionization potential I_{pa}	4.6791	4.6474	4.6171	4.5882	4.5606	4.5341
vertical ionization potential I_{pv}	4.91	4.63	4.6323	4.6021	4.5732	4.5454
LUMO	-3.02	-3.27	-3.123	-3.1499	-3.1757	-3.2003
	$C_{260}H_{20}$	$C_{270}H_{20}$	$C_{280}H_{20}$	$C_{290}H_{20}$	$C_{300}H_{20}$	$C_{310}H_{20}$
LUMO-HOMO gap Δ	0.54	0.5055	0.4724	0.4404	0.4095	0.3797
absolute hardness η	1.84	1.783	1.727	1.674	1.623	1.573
adiabatic ionization potential I_{pa}	4.5086	4.484	4.4604	4.4376	4.4155	4.3942
vertical ionization potential I_{pv}	4.5187	4.4931	4.4683	4.4445	4.4214	4.3991
LUMO	-3.224	-3.2467	-3.2686	-3.2896	-3.31	-3.3296

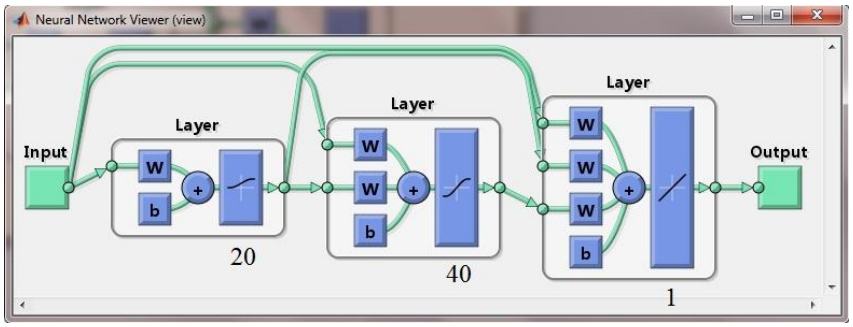

Figure 4. The CFFBP-NN method used to calculate λ_h for **1-30**.

Table 8. The *"Output"* data for [SWCNT(5,5)-Armchair-C_nH_{20}] (n=200-310) **19-30** of the hole reorganization energy (λ_h) by the neural network model (20 LOGSIG, 40 TANSIG, 1 PURELIN).

	$C_{200}H_{20}$	$C_{210}H_{20}$	$C_{220}H_{20}$	$C_{230}H_{20}$	$C_{240}H_{20}$	$C_{250}H_{20}$
hole reorganization energy λ_h	0.051	0.023	0.045	0.047	0.050	0.053
	$C_{260}H_{20}$	$C_{270}H_{20}$	$C_{280}H_{20}$	$C_{290}H_{20}$	$C_{300}H_{20}$	$C_{310}H_{20}$
hole reorganization energy λ_h	0.055	0.058	0.061	0.064	0.066	0.070

To calculate the λ_e, the cascade-feed forward back-propagation neural network (CFFBP-NN) method that was used for training was utilized (Figure 3). As shown in Figure 3, each of the input data values of the network consisted of a (6x1) vector, and the output value of the network for each vector of input was the electron reorganization energy (λ_e).

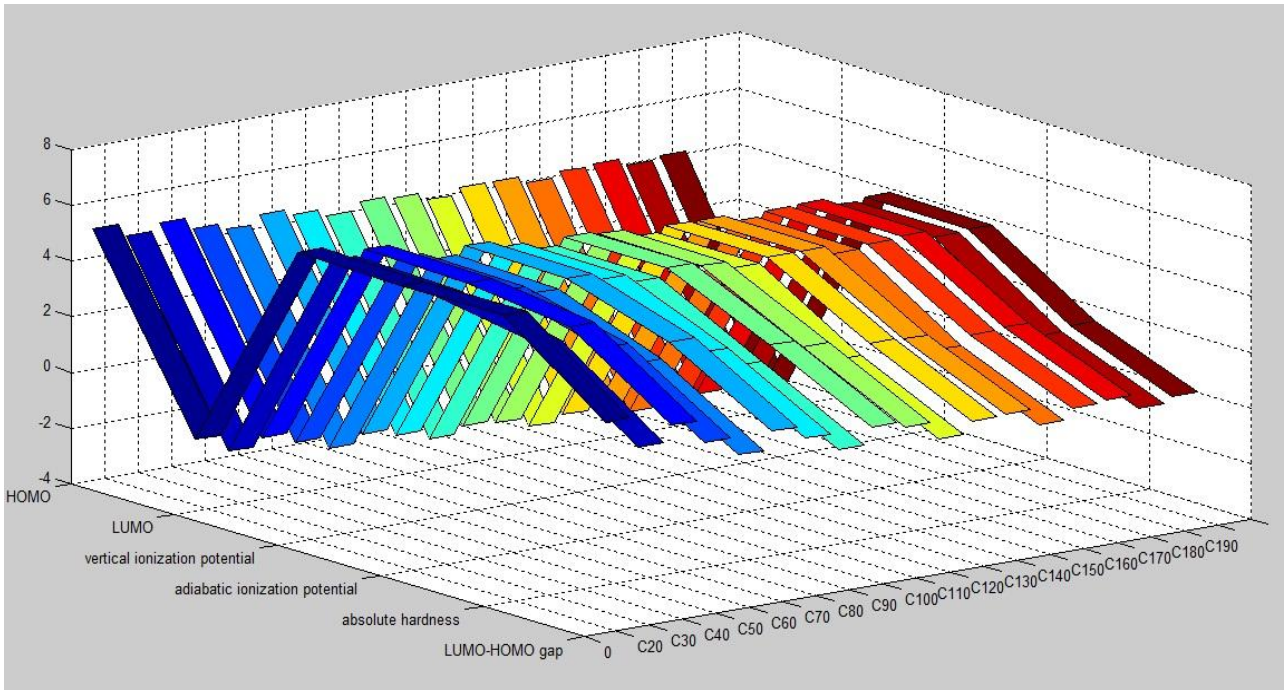

Figure 5. The three dimentional relationship among the selected *"Input"* data of [SWCNT(5,5)-Armchair-C_nH_{20}] (n=20-190) **1-18** for calculation the electron reorganization energy (λ_e) by the neural network model. See Table-1.

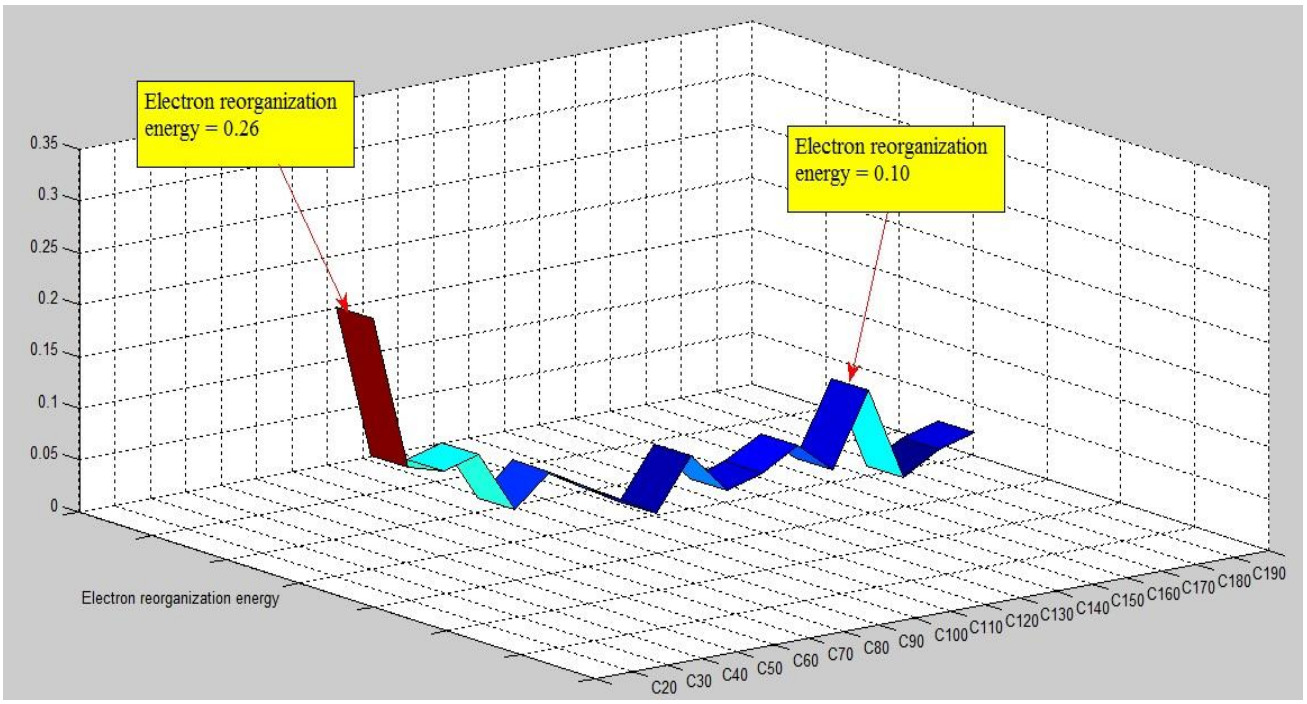

Figure 6. The three dimentional relationship among the selected *"Target"* data of electron reorganization energy (λ_e) by the neural network model for [SWCNT(5,5)-Armchair-C_nH_{20}] (n=20-190) **1-18**. See Table-2.

The network used to calculate the λ_h value was the cascade-feed forward back-propagation neural network (CFFBP-NN), which was also used for training (Figure 4). Figure 4 shows that each of the input data values of the network consisted of a (5x1) vector and that the output data values of the network for each input vector was a hole reorganization energy (λ_h) value.

Using two CFFBP-NN models, it was possible to derive a good approximation to extend the formulas for the electron reorganization energy (λ_e) and the hole reorganization energy (λ_h) for the [SWCNT(5,5)-armchair-C_nH_{20}] (n=20-310) 1-30. Herein, the extension of the λ_e and λ_h data are reported for the first time for [SWCNT(5,5)-armchair-C_nH_{20}] (n=200-310) 19-30. Tables 2 to 4 for λ_e and Tables 6 to 8 for λ_h show the data for the CFFBP-NN process. Figure 5 demonstrates the three dimensional relationship between the selected *"Input"* data of the [SWCNT(5,5)-Armchair-C_nH_{20}] (n=20-190) 1-18 for the calculations of the electron reorganization energy (λ_e) by the CFFBP-NN model. Figure 5 is related to Table-1.

Figure 6, which is related to Table 2, shows a three dimensional relationship for the *"Target"* data of the electron reorganization energy (λ_e) calculated by the neural network model for the [SWCNT(5,5)-Armchair-C_nH_{20}] (n=20-190) 1-18. Figure 7 illustrates the three dimensional relationship among the selected *"Test"* data for the [SWCNT(5,5)-Armchair-C_nH_{20}] (n=200-310) 19-30 of the electron reorganization energy (λ_e) by the neural network model (45 LOGSIG, 50 LOGSIG, and 1 PURELIN). Table 3 is related to Figure 7.

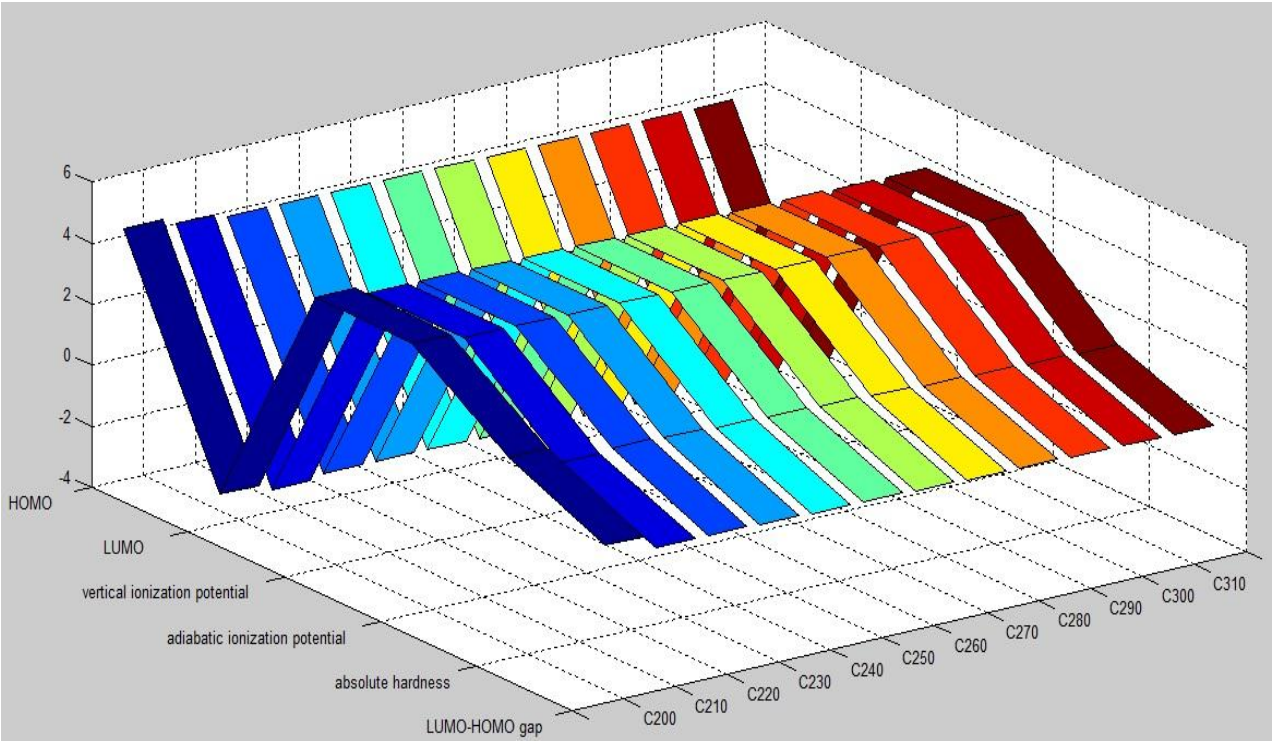

Figure 7. The three dimentional relationship among the selected *"Test"* data for [SWCNT(5,5)-Armchair-C_nH_{20}] (n=200-310) **19-30** of the electron reorganization energy (λ_e) by the neural network model (45 LOGSIG, 50 LOGSIC, 1 PURELIN). See Table-3.

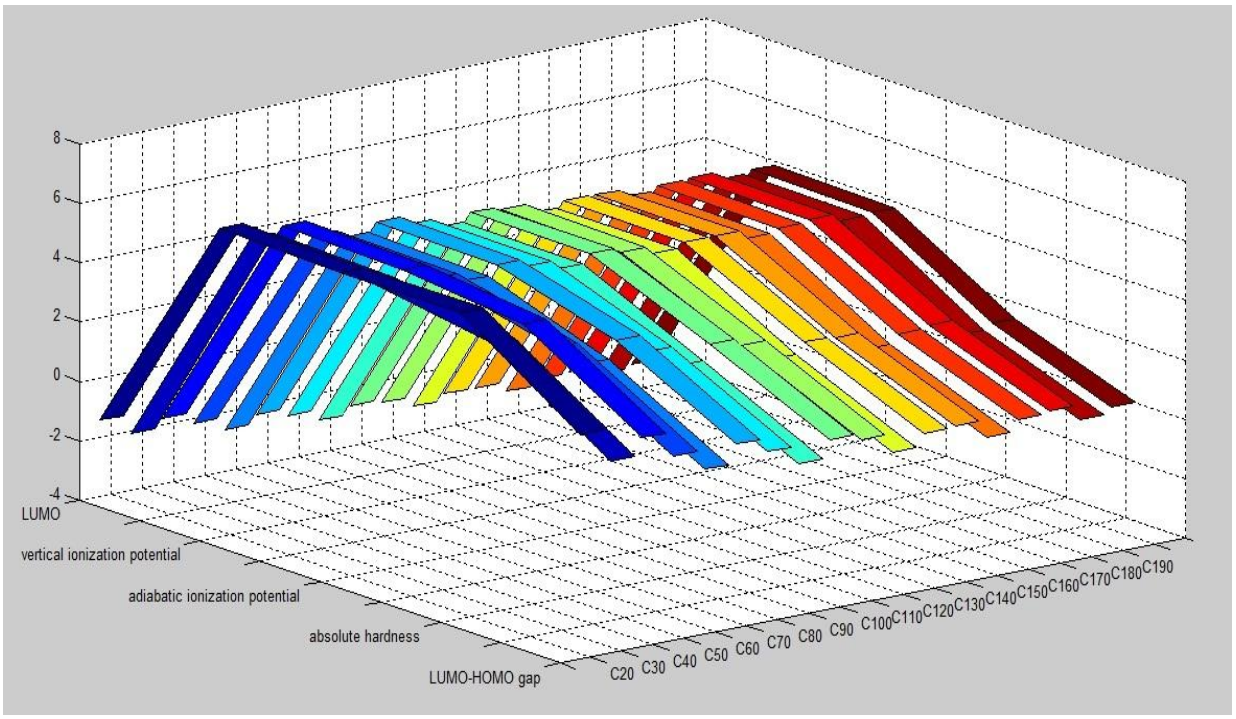

Figure 8. The three dimentional relationship among the selected*"Input"* data of [SWCNT(5,5)-Armchair-C_nH_{20}] (n=20-190) **1-18** for calculation the hole reorganization energy (λ_h) by the neural network model. See Table-5.

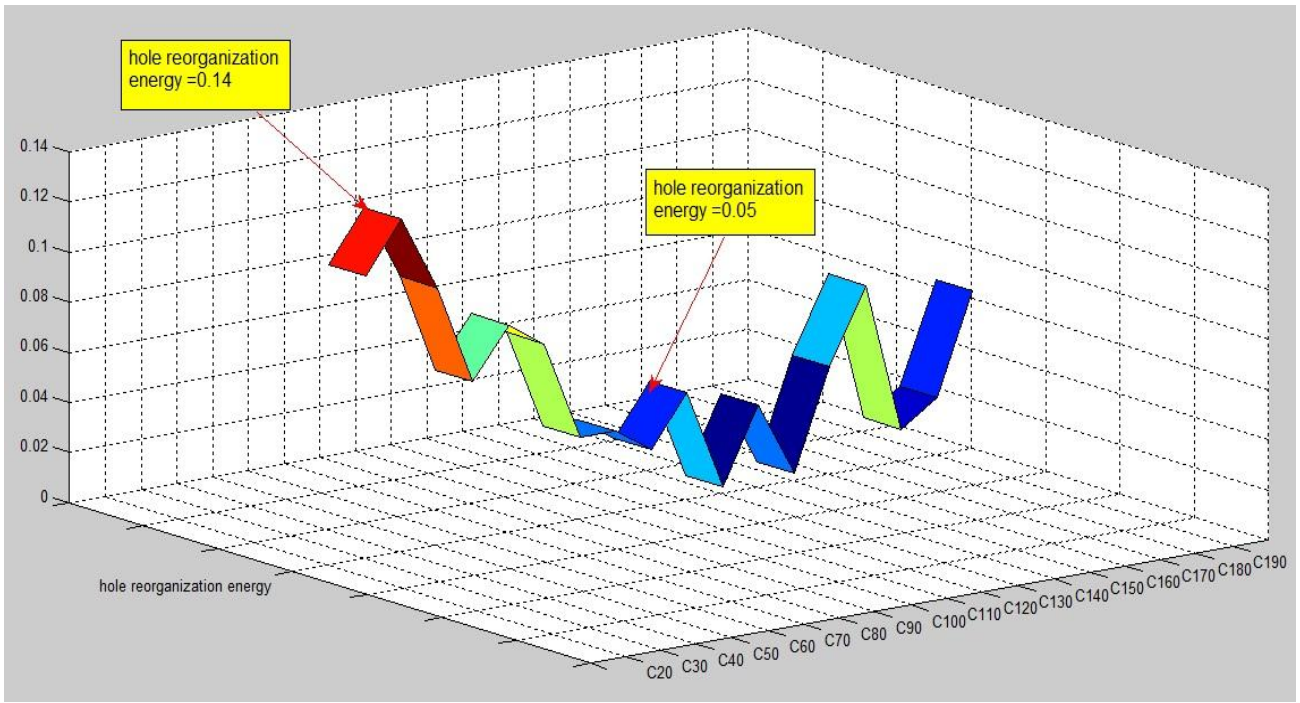

Figure 9. The three dimentional relationship among the selected *"Target"* data of hole reorganization energy (λ_h) by the neural network model for [SWCNT(5,5)-Armchair-C_nH_{20}] (n=20-190) **1-18**. See Table-6.

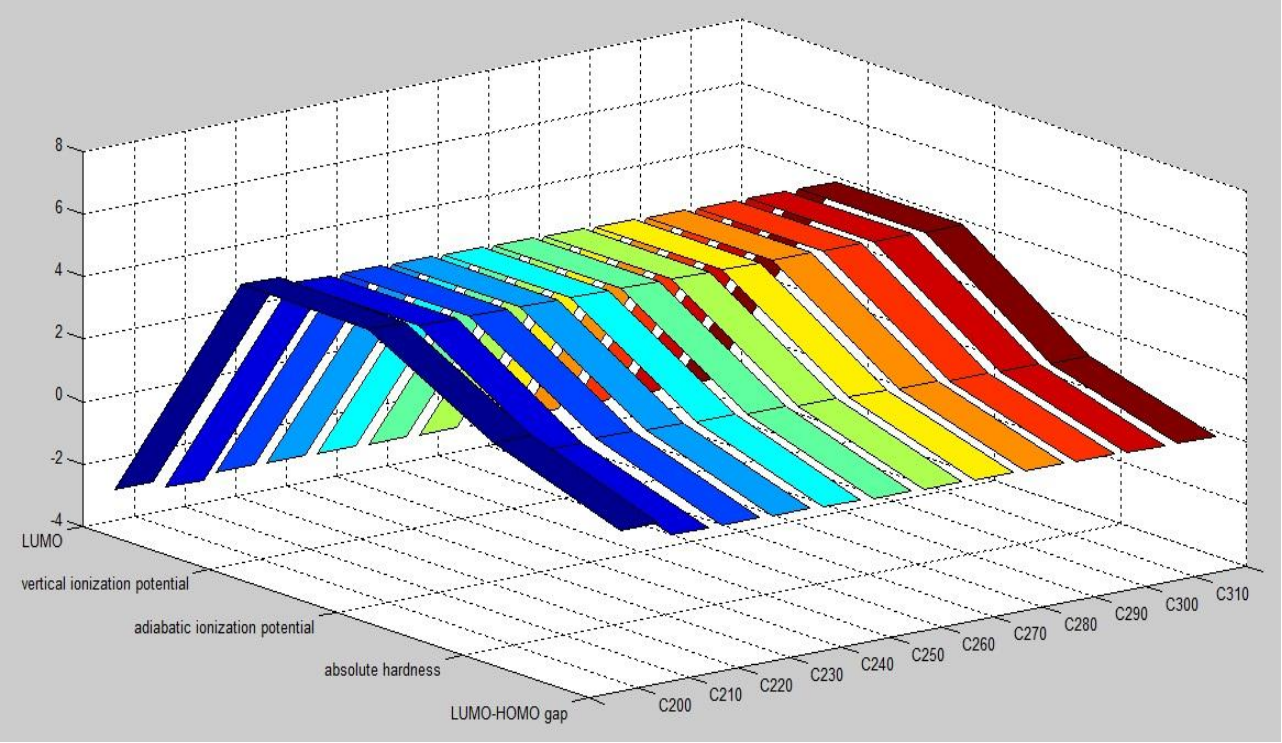

Figure 10. The three dimentional relationship among the selected *"Test"* data for [SWCNT(5,5)-Armchair-C_nH_{20}] (n=200-310) **19-30** of the hole reorganization energy (λ_h) by the neural network model (20 LOGSIG, 40 TANSIG, 1 PURELIN). See Table-7.

Figure 8 displays the three dimensional relationship for the selected *"Input"* data of the [SWCNT(5,5)-Armchair-C_nH_{20}] (n=20-190) 1-18 for the calculations of the hole reorganization energy (λ_h) by the CFFBP-NN model (see Table 5). Figure 9, which is related to Table 6, shows a three dimensional relationship among the *"Target"* data for the hole reorganization energy (λ_h) by the CFFBP-NN model for the [SWCNT(5,5)-Armchair-C_nH_{20}] (n=20-190) 1-18. Figure 10 displays the three dimensional relationship for the selected *"Test"* data of the [SWCNT(5,5)-Armchair-C_nH_{20}] (n=200-310) 19-30 of the hole reorganization energy (λ_h) by the neural network model (20 LOGSIG, 40 TANSIG, and 1 PURELIN) (see Table 7).

Using the cascade-feed forward back-propagation neural network (CFFBP-NN) model, it was possible to calculate the electron reorganization energy (λ_e) and the hole reorganization energy (λ_h) for [SWCNT(5,5)-Armchair-C_nH_{20}] (n=200-310) 19-30 in accordance with the Marcus theory.

Good correlations were established for the number of carbon atoms (C_n), the LUMO-HOMO gap (ΔE in eV), absolute hardness (η), adiabatic ionization potential (I_{pa}), vertical ionization potential (I_{pv}), the hole reorganization energy (λ_h), and the LUMO and HOMO energies with the electron reorganization energy (λ_e) in the applied CFFBP-NN model for [SWCNT(5,5)-Armchair-C_nH_{20}] (n=20-190) of 1-18; thus, it was possible to use these values to calculate the electron reorganization energy (λ_e) and the hole reorganization energy (λ_h) for [SWCNT(5,5)-Armchair-C_nH_{20}] (n=200-310) 19-30.

The results of the CFFBP-NN model were extended towards the calculations of the λ_e and λ_h of $C_{200}H_{20}$ up to $C_{310}H_{20}$ in the [SWCNT(5,5)-armchair-C_nH_{20}] 19-30. With the appropriate CFFBP-NN

model operations, it was possible to calculate the λ_e and λ_h in 1-18 and 19-30. The values of λ_e and λ_h reported herein for 19-30 have neither been previously measured nor reported.

4. CONCLUSIONS

Nanoscale structures of carbon display an attractive variation of structural characteristics, and many useful forms, such as for building computers, microchips, sensors, actuators and machines, have been synthesized and identified. An important type of nanoscale structures is called a single wall carbon nanotube (SWCNT). The number of carbon atoms (C_n) and the LUMO-HOMO gap (ΔE in eV), absolute hardness (η), adiabatic ionization potential (I_{pa}), vertical ionization potential (I_{pv}), LUMO and HOMO energies of 1-18 show a strong correlation with the values of the electron reorganization energy (λ_e) and the hole reorganization energy (λ_h) in the (5,5) armchair SWCNT 1-18 and 19-30; these are important factors obtained for these materials using the cascade-feed forward back-propagation neural network (CFFBP-NN) method. The values of λ_e and λ_h were calculated using the CFFBP-NN model based on the Marcus theory for [SWCNT(5,5)-Armchair-C_nH_{20}] (n=200-310) 19-30 nanostructures. Using this model and the associated methods, it was possible to calculate the *electron reorganization energy* (λ_e) and the hole reorganization energy (λ_h) of this family of compounds 1-30 in a simple manner and with good approximation.

ACKNOWLEDGMENTS
The author gratefully acknowledges his colleagues in the Chemistry Department of The University of New England (UNE)-Australia for their useful suggestions.

References

1. Z. Zhou, M. Steigerwald, M. Hybertsen, L. Brus, R.A. Friesner, *J. Am. Chem. Soc.*, 126 (2004) 3597-3607 (and the literature cited therein).
2. J. W. Mintmire, B. I. Dunlap, C. T. White, *Phys. Rev. Lett.*, 68 (1992) 631.
3. R. Saito, M. Fujita, G. Dresselhaus, M. S. Dresselhaus, *Phys. Rev. B*, 46 (1992) 1804.
4. N. Tezuka, T. Umeyama, S. Seki, Y. Matano, M. Nishi, K. Hirao and H. Imahori, *J. Phys. Chem. C*, 114 (2010) 3235–3247.
5. R. H. Baughman, A. A. Zakhidov, W. A. de Heer, *Science*, 297 (2002) 787.
6. H. J. Dai, *Acc. Chem. Res.*, 35 (2002) 1035.
7. M. Ouyang, J. L. Huang, C. M. Lieber, *Acc. Chem. Res.*, 35 (2002) 1018.
8. P. Avouris, Z. H. Chen, V. Perebeinos, *Nat. Nanotechno*., 2 (2007) 605.
9. E. Katz, I. Willner, *Chem. Phys. Chem.*, 5 (2004) 1084.
10. D. M. Guldi, G. M. A. Rahman, F. Zerbetto, M. Prato, *Acc. Chem. Res.*, 38 (2005) 871.
11. P. V. Kamat, *J. Phys. Chem. C*, 111 (2007) 2834.
12. P. Avouris, M. Freitag, V. Perebeinos, *Nat. Photonics*, 2 (2008) 341.
13. T. Umeyama, H. Imahori, *Energy Environ. Sci.*, 1 (2008) 120.
14. V. Sgobba, D. M. Guldi, *Chem. Soc. Rev.*, 38 (2009) 165.
15. H. Ago, K. Petritsch, , M. S. P. Shaffer. A. H. Windle, R. H. Friend, *Adv. Mater.*, 11 (1999) 1281.

16. A.Star, J. F. Stoddart, D. Steuerman, M. Diehl, A. Boukai, E. W. Wong, X. Yang, S. W. Chung , H. Choi, J. R. Heath, *Angew. Chem. Int. Ed.*, 40 (2001) 1721.
17. E. Kymakis, G. A. J. Amaratunga, *Appl. Phys. Lett.*, 80 (2002) 112.
18. E. Kymakis, I. Alexandrou, G. A. J. Amaratunga, *J. Appl. Phys.*, 93 (2003) 1764.
19. S. Barazzouk, S. Hotchandani, K. Vinodgopal, P. V. Kamat, *J. Phys. Chem. B*, 108 (2004) 17015.
20. T. Hasobe, S. Fukuzumi, P. V. Kamat, *J. Phys. Chem. B*, 110 (2006) 25477.
21. D. S. Hecht, R. J. A. Ramirez, M. Briman, E. Artukovic, K. S. Chichak, J. F. Stoddart, G. Grüner, *Nano Lett.*, 6 (2006) 2031.
22. L. Hu, Y. L. Zhao, K. Ryu, C. Zhou, J. F. Stoddart, , G. Grüner, *Adv. Mater.*, 20 (2008) 939.
23. T. Umeyama, M. Fujita, N. Tezuka, N. Kadota, Y. Matano, K. Yoshida, S. Isoda, H. Imahori, *J. Phys. Chem. C*, 111 (2007) 11484.
24. D. M. Guldi, G. M. A. Rahman, M. Prato, N. Jux, S. Qin, W.Ford, *Angew. Chem. Int. Ed.*, 44 (2005) 2015.
25. G. M. A. Rahman, D. M. Guldi, R. Cagnoli, A. Mucci, L. Schenetti, L. Vaccari, M. Prato, *J. Am. Chem. Soc.*, 127 (2005) 10051.
26. G. M. A. Rahman, A. Troeger, V. Sgobba, D. M. Guldi, N. Jux, D. Balbino, M. N. Tchoul, W. T. Ford, A. Mateo-Alonso, M. Prato, *Chem. Eur. J.*, 14 (2008) 8837.
27. L. Sheeney-Haj-Ichia, B. Basnar, I. Willner, *Angew. Chem. Int. Ed.*, 44 (2005) 78.
28. S. Campidelli, B. Ballesteros, A. Filoramo, D. D. Diaz, G. D. L. Torre, T. Torres, G. M. A. Rahman, C. Ehli, D. Kiessling, F. Werner, V. Sgobba, D. M. Guldi, C. Cioffi, M. Prato, J. P. Bourgoin, *J. Am. Chem. Soc.*, 130 (2008) 11503.
29. T. Arai, S. Nobukuni, A. S. D. Sandanayaka, O. Ito, *J. Phys. Chem. C*, 113 (2009) 14493.
30. D. Srivastava, M. Menon, K. Cho, *Compu. Sci. & Eng.*, 3 (2001) 42-55 (and the literature cited therein).
31. O. Lourie, D.M. Cox, H.D. Wagner, *Phys. Rev. Letters*., 81 (1998) 1638-1641.
32. S. Nagase, K. Kobayashi, *J. Chem. Soc. Chem. Commun*., 16 (1994) 1837-1838.
33. D. Dubois, K.M. Kadish, S. Flanagan, L. J. Wilson, *J. Am. Chem. Soc.*, 113(10) (1991) 7773-7774.
34. Q. Xie, E. Pérez-Cordero, L. Echegoyen, *J. Am. Chem. Soc*., 114 (1992) 3978-3980.
35. J.W. Mintmire, B.I. Dunlap, C.T. White, *Phys. Rev. Lett*., 68 (1992) 631-634.
36. Q. Li, F. Wudl, C. Thilgen, R.L. Whetten, F. Diederich, *J. Am. Chem. Soc*., 114(10) (1991) 3994-3996.
37. J.S. Arellano, L.M. Molina, A. Rubio, M.J. Lopez, J.A. Alonso, *J. Chem. Phys*., 117(5) (2002) 2281-2288.
38. D. Srivastava, S. Barnard, *"Molecular dynamics simulation of large scale carbon nanotubes on a shared memory architecture," Proc. IEEE Supercomputing 97, IEEE Computer Soc. Press, Los Alamitos, Calif.,* 1997.
39. B.I. Yakobson, P. Avouris, *Mechanical properties of carbon nanotubes.* Springer-Verlag: Berlin., (2001) 293.
40. P. Avouris, *Acc of Chem Research*., 35(12) (2002) 1026-1034.
41. M.S. Dresselhaus, G. Dresselhaus, P. Avouris, *Carbon nanotubes: Synthesis, Structure, Properties and Applications.* Eds. Springer-Verlag: Berlin., 2001.
42. Special issue on carbon nanotubes; *Physics World*, June, 13(6) (2000). *(Cross ref.)*.
43. M.S. Dresselhaus, G. Dresselhaus, R. Saito, *Phys. Rev*. B, 45(11) (1992) 6234-6242.
44. R. Barnett, E. Demler, E. Kaxiras, *Solid State Comm*., 135(5) (2005) 335-339.
45. A.Sygula, F. R. Fronczek, R. Sygula, P. W. Rabideau and M. M. Olmstead, *J. Am. Chem. Soc*., 129 (2007) 3842-3843.
46. M.V. Diudea, *Fulle Nanot Carb Nanost(FNCN)*, 10(4) (2002) 273-292.
47. M.V. Diudea, *J. Chem. Inf. Model.*, 45 (2005) 1002-1009.

48. M.V. Diudea, Polyhex tori originating in square tiled tori, in: Diudea MV, Ed., *Nanostructures, Novel architecture, NOVA.*, (2005) 111-126.
49. D. Srivastava, S.N. Atluri, *CMES.*, 3(5) (2002) 531-538.
50. A.A. Taherpour, *Chem. Phys. Lett*., 469 (2009) 135-139.
51. A.A. Taherpour, *Fulle Nanot Carb Nanost(FNCN).*, 16(3) (2008) 196–205.
52. A.A. Taherpour, *Fulle Nanot Carb Nanost(FNCN).*, 15(4) (2007) 279–289.
53. A.A. Taherpour, F. Shafiei, *J. Mol. Struct. THEOCHEM*, 726(1-3) (2005)183-188.
54. A.A. Taherpour, *J. Phys. Chem. C*, 113 (2009) 5402–5408.
55. A.A. Taherpour, *Phosphorus, Sulfur, and Silicon*., 185 (2010) 422–432.
56. A.A. Taherpour, *Chem. Phys. Lett.*, 483 (2009) 233-240.
57. A.A. Taherpour and M. Maleki, *Anal. Lett.*, 43(4) (2010) 658-673.
58. P.J. Hansen, P. Jurs, *J. Chem. Edu.*, 65(7) (1988) 574-580 (and the literature cited therein).
59. H. Hosoya, Bull. *Chem. Soc. Jpn.*, 44 (1971) 2332-2339.
60. M. Randić, *Acta. Chim. Slov.*, 45(3) (1998) 239-252.
61. G. Rücker, C. Rücker, *J. Chem. Inf. Cmput. Sci*., 39(5) (1999) 788-802.
62. H. Wiener, *J. Am. Chem. Soc.*, 69(1) (1947) 17-20.
63. The website of L. Dunsch, IFW-Dresden-Germany: http://www.ifw-dresden.de/institutes/iff/research/Carbon/fullerenes/introduction.
64. http://en.wikipedia.org/wiki/Fullerene
65. Y.P. Du, Y.Z. Liang, B.Y. Li, C.J. Xu, *J. Chem. Inf. Cmput. Sci.*, 42(5) (2002) 993-1003.
66. M. Randić, *J. Am. Chem. Soc*., 97(23) (1975) 6609-6615.
67. S.D. Bolboaca, L. Jantschi, *Int. J. Mol. Sci.*, 8(4) (2007) 335-345.
68. Z. Slanina, F. Uhlik, S.L. Lee, E. Osawa, *MATCH. Commun. Math. Comput. Chem*., 44 (2001) 335-348.
69. R.A. Marcus, *Rev. Modern Physics*., 65(3) (1993) 599-610.
70. M. Andrea Marcus Theory for Electron Transfer a short introduction *MPIP. J. Club-Mainz.*, 29 (2008) 29.
71. P.F. Barbara, *J. Phys. Chem*., 100 (1996) 13148-13161.
72. M.D. Newton, *Chem. Ren*., 91 (1991) 767-792.
73. J. Jortner, J. and K.F. Freed, *J. Chem. Phys*., 52 (1970) 6272-6291.
74. R.A. Marcus, *J. Chem. Phys*., 43 (1965) 679.
75. R. A. Marcus, N. Sutin, *Biochim. Biophys. Acta.*, 811 (1985) 265.
76. M.G. Kuzmin, *XVIIth IUPAC Symposium on Photochemistry*, Dresden, German, July 22-27 (2000) Book of Abstracts, p. 372.
77. R. A. Marcus, *Annu. Rev. Phys. Chem.*, 15 (1964) 155.
78. Marcus, R. A. *Angew. Chem., Int. Ed. Engl.*, 32 (1993)1111.
79. S. Frank Texas Instruments, Incorporated "*Neural Network Classification of Photoemission Spectra*," IEEE 02CH37320.4Oh Annual International Reliability Physics Symposium, Dallas, Texas, August., (2002) 205-209.
80. K. Ohkubo, H. Imahori, J. Shao, Z. Ou, K. M. Kadish, Y. Chen, G. Zheng, R. K. Pandey, M. Fujitsuka, O. Ito and S. Fukuzumi, *J. Phys. Chem. A*, 106 (2002) 10991-10998.
81. T. Okada, M. Shirakawa, Y. Sakata, *Chem. Phys. Lett*., 263 (1996) 545.
82. N. V. Tkachenko, C. Guenther, H. Imahori, K. Tamaki, Y. Sakata, S. Fukuzumi, H. Lemmetyinen, *Chem. Phys. Lett.*, 326 (2000) 344.
83. H. Imahori, K. Tamaki, H. Yamada, K. Yamada, Y. Sakata, Y. Nishimura, I. Yamazaki, M. Fujitsuka, O. Ito, *Carbon*, 38 (2000) 1599.
84. H. Imahori, N.V. Tkachenko, V. Vehmanen, K. Tamaki, H. Lemmetyinen, Y. Sakata, S. Fukuzumi, *J. Phys. Chem. A*, 105 (2001) 1750.
85. V. Vehmanen, N. V. Tkachenko, H. Imahori, S. Fukuzumi, H. Lemmetyinen, *Spectrochim. Acta, Part A*, 57 (2001) 2229.

86. H. Imahori, H. Yamada, D. M. Guldi, Y. Endo, A. Shimomura, S. Kundu, K. Yamada, T. Okada, Y. Sakata, S. Fukuzumi, *Angew. Chem. Int. Ed.*, 42 (2002) 2344.
87. D. M. Guldi, K. D. Asmus, *J. Am. Chem. Soc.*, 119 (1997) 5744.
88. H. Imahori, K. Tamaki, D. M. Guldi, C. Luo, M. Fujitsuka, O. Ito, Y. Sakata, S. Fukuzumi, *J. Am. Chem. Soc.*, 123 (2001) 2607.
89. C. Luo, D. M. Guldi, H. Imahori, K. Tamaki, Y. Sakata, *J. Am. Chem. Soc.*, 122 (2000) 6535.
90. K. Yamada, H. Imahori, Y. Nishimura, I. Yamazaki, Y. Sakata, *Chem. Lett.*, (1999) 895.